Nanotechnology Perceptions
ISSN 1660-6795
www.nano-ntp.com

Unveiling the Structural, Thermal, and Optical Studies on 7BA Liquid Crystal Dispersed with Dysprosium-Doped Lithium Zinc Phosphate Phosphor Nanoparticles

R. Trisanjya[1], Ch. Ravi Shankar Kumar[2], P. Jayaprada[3], RKNR Manepalli[1]

[1]LCNC Laboratory, Department of Physics, Andhra University, Visakhapatnam-530003, India
[2]Department of Physics, School of Science, GITAM University, Visakhapatnam-530045, India
[3]Department of Physics, Dhanekula Institute of Engineering and Technology, Vijayawada - 521139, India
Email: trisanjyareddipalli.rs@andhrauniversity.edu.in

This study explores the structural, thermal, and optical characteristics of p-n-heptyl benzoic acid (7BA) liquid crystal infused with dysprosium-doped lithium zinc phosphate ($Li_4Zn(PO_4)_2:Dy^{3+}$) phosphor nanoparticles at concentrations of 1.5 wt%, 2.5 wt%, and 3.5 wt%. The $Li_4Zn(PO_4)_2:Dy^{3+}$ nanoparticles were synthesized via a combustion method and characterized using X-ray diffraction (XRD), confirming their incorporation into the 7BA matrix. Scanning electron microscopy (SEM) and energy-dispersive X-ray spectroscopy (EDS) demonstrated the uniform dispersion of the nanoparticles within the liquid crystal structure.

UV-visible spectroscopy revealed a increase in the energy bandgap of 7BA from 4.04 eV to 4.13 eV as the nanoparticle concentration increased. Differential scanning calorimetry (DSC) and polarized optical microscopy (POM) were employed to analyze the phase transition temperatures and textures of the nanocomposites, while Fourier-transform infrared spectroscopy (FTIR) identified functional groups and highlighted subtle shifts in regions corresponding to C=O, C=C, and C-H bond stretching as nanoparticle concentrations varied.

This integration of $Li_4Zn(PO_4)_2:Dy^{3+}$ nanoparticles into the 7BA liquid crystal

matrix demonstrates their potential to enhance and customize liquid crystal properties, opening new avenues for advanced display technologies and optoelectronic applications**.**
Keywords: Liquid crystalline 7-BA, Dysprosium, XRD, SEM, FTIR, DSC, POM.

1. Introduction

Liquid crystals (LCs) have profoundly transformed modern technology, establishing themselves as indispensable materials across various scientific and industrial domains. They serve as the foundation for high-resolution displays, E-books, and biomedical imaging systems such as hyperspectral imaging and ophthalmology. Additionally, their tunable optical properties make them essential in precision instruments, including wave plates, retarders, rotators, and polarization generators. Furthermore, LCs play a crucial role in sophisticated optical processing systems, continuously pushing the boundaries of innovation and application [1].

In recent years, nanomaterials have emerged as a cornerstone in the advancement of nanoscience and nanotechnology[2]. Their exceptional electronic, optical, magnetic, and chemical properties arising from their nanoscale dimensions have unlocked a multitude of possibilities for cutting-edge research and industrial applications of particular significance are their pronounced electro-optic and thermo-optic effects, attributed to their high birefringence and substantial dielectric anisotropy [3,4]. These unique characteristics position nanomaterials as key enablers in the development of advanced functional materials.

The strategic incorporation of nanoparticles (NPs) into liquid crystal systems has demonstrated remarkable enhancements in their optical and electrical performance. Metal nanoparticle-infused LCs, in particular, exhibit significant improvements in thermo-optic and electro-optic responses. Various categories of nanoparticles including semiconducting, ferroelectric, metallic, inorganic, carbon-based, and ferro-nematic have shown substantial potential in refining the electro-optic behavior of LC-based devices [5-10]. When introduced into nematic LCs, nanoparticles induce profound modifications in their structural parameters, influencing attributes such as shape, size, texture, and phase transition temperatures [11,12]. Among rare-earth elements, dysprosium (Dy^{3+}) stands out due to its distinct multi-energy levels and emission bands, covering blue, yellow, and faint red wavelengths. These attributes make Dy^{3+} ions highly suitable for applications in artificial photosynthesis and high-purity luminescent systems. The choice of an appropriate host material plays a pivotal role in achieving stable and efficient white light emission from Dy^{3+} ions.

Phosphate materials have gained significant attention as host matrices for rare-earth ion doping due to their environmentally friendly composition, cost-effectiveness, and adaptable PO_4 tetrahedral coordination. Their extensive use in display panel technologies underscores their commercial significance. Furthermore, phosphate-based luminescent hosts, when doped with alkali and/or alkaline earth metals, exhibit broad bandgaps (Eg) in the ultraviolet region and moderate phonon energy, leading to enhanced luminescence efficiency [13,14]. The doping of LCs with rare-earth nanoparticles, such as Dy^{3+}, results in notable alterations to their electro-

optical properties, including variations in their dielectric constant [15,16]. Comprehensive investigations utilizing anisotropic liquid crystal films, analyzed via spectroscopic ellipsometry, have provided insights into the wavelength-dependent electro-optical behavior of these materials [17-20].

The rapid advancement of emerging technologies necessitates the development of novel liquid crystals with tailored properties. However, the chemical synthesis of new LC compounds remains a costly, time-consuming, and intricate process. A more viable approach lies in modifying existing LC systems by incorporating small amounts of functional additives. The introduction of nanoparticles in concentrations as low as 0.01 to 0.1 wt% has been shown to induce substantial changes in LC behavior, offering a cost-effective alternative for material optimization [21,22].

The transition to solid-state lighting represents a crucial step toward replacing conventional illumination systems with energy-efficient, cost-effective, and environmentally sustainable solutions. White light-emitting diodes (LEDs) are at the forefront of this transformation, yet further refinements are required to achieve tunable and high-efficiency color outputs. These LEDs are typically fabricated using blue or near-ultraviolet excitation chips in conjunction with phosphor materials. Rare-earth-activated phosphors play an instrumental role in numerous applications, including bioimaging, temperature sensing, optical heating, and bio-thermal treatments, owing to their high emission intensity and narrow bandwidth characteristics. Among these, Dy^{3+} ions exhibit distinct advantages due to their multiple energy levels and emission bands across blue, yellow, and faint red wavelengths. Their relevance in artificial photosynthesis and their superior color purity further highlight their importance in advanced luminescent applications. The choice of a suitable host matrix is crucial for ensuring efficient and uniform white light emission from Dy^{3+} ions [23].

This study investigates the integration of dysprosium-doped phosphor nanoparticles within a liquid crystal matrix, specifically p-(n-heptyl) benzoic acid (7BA). The nanoparticles were incorporated at three different weight concentrations 1.5 wt%, 2.5 wt%, and 3.5 wt% using a combination of magnetic stirring and sonication bath dispersion techniques. The primary objective of this research is to evaluate the structural, electrical, and optical properties of 7BA liquid crystals doped with Dy^{3+}-activated phosphor nanoparticles, thereby contributing to the development of next-generation electro-optic devices.

2.Materials and methods:

2.1 Synthesis of Dy^{3+} doped lithium zinc phosphor nanoparticles

In this study, DLZP-NPs were synthesized via combustion method [24]. The combustion technique offers advantages over traditional solid-state reactions, including reduced processing temperatures and improved phase purity. The ingredients such as 3.21g of lithium carbonate, 1.772 g of zinc oxide and 5.002 g of ammonium phosphate were grinded well in agate mortar and then mixed with 0.373 g of dysprosium oxide (0.1 mole). The complex mixture was grinded well. Further, 3 g of urea as fuel and 0.3 g of boric acid as flux were added. The complex mixture was placed in auto clave and then heated in high temperature chamber at 800^{o}C about 1h. The obtained resultant composite mixture consists of DLZP-NPs.

2.2 Synthesis of 7-BA with DLZP-NPs

7-BA, acquired from Sigma-Aldrich (St. Louis, MO, USA), was employed without undergoing supplementary purification procedures. A series of 7-BA with the dispersion of DLZP-NPs with varying concentrations (1.5-3.5 wt%) were prepared via a solution-based method. Typically, 100 mg of 7-BA was dissolved in 5 mL of ethyl alcohol. The solution was then stirred at 600 rpm for 1 h at 60°C using a magnetic stirrer. Subsequently, 1.5 wt% of DLZP-NPs was added to the solution, and the mixture was further stirred about 2-3 h and then placed in ultra-sonicator bath. The solvent was then evaporated, resulted in the formation of 7-BA with Dy^{3+} doped phosphor nanocomposite material. This procedure was replicated for other concentrations 2.5 and 3.5 wt%. The structural, morphological, thermal and optical properties of the liquid crystal samples were comprehensively analyzed using a suite of advanced characterization techniques.

3. Results and Discussion:

3.1: XRD Studies:

Powdered X-ray diffraction (XRD) analysis was conducted using a Bruker D8-Advance diffractometer (Model No: 216730). The XRD patterns for Dy^{3+}-doped phosphor nanoparticles, synthesized at a concentration of 2.5 wt%, are illustrated in Fig. 1(a). These nanoparticles, when dispersed in 7BA, exhibit prominent diffraction peaks at 2θ values of 9.9°, 12.9°, 14.9°, 20.0°, and 24.5°. These peaks correspond to the (h k l) planes (0 1 1), (0 2 1), (1 1 1), (0 4 1), and (1 3 2), respectively, as indexed in the JCPDS database (Card No: 00-720-0940). This unequivocally confirms the successful incorporation of Dy^{3+} ions into the phosphor nanoparticles within the 7BA matrix.

The crystallite size of the Dy^{3+}-doped phosphor nanoparticles was determined using the Debye-Scherrer equation, supported by Unit Cell software, yielding a calculated size of 88.92 nm [25].

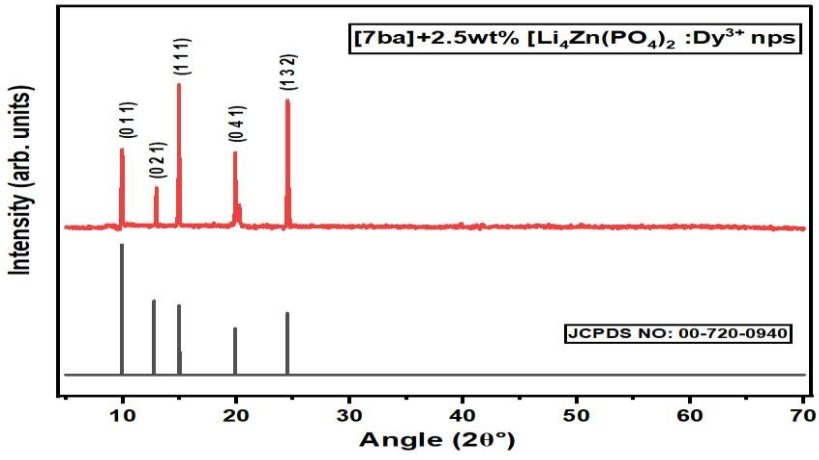

Fig 1 (a) XRD Analysis of 7BA dispersed in 2.5wt% $Li_4Zn(PO_4)_2$:Dy^{3+} phosphor nps

3.2 SEM Analysis:

Scanning Electron Microscopy (SEM) was employed to explore the structural properties of the liquid crystal nano-composite, $Li_4Zn(PO_4)_2:Dy^{3+}$, providing insights into nanoparticle size, shape, and distribution within the 7BA liquid crystal matrix [26,27]. These characteristics play a pivotal role in influencing the electro-optical performance of the material, making it a promising candidate for advanced display technologies [28]. SEM's high-resolution imaging capability enabled detailed visualization of the nanoparticle morphology and surface architecture. Complementarily, Energy Dispersive Spectroscopy (EDS) was utilized to analyze the elemental composition and surface features.

Figures 2(a) and 2(b) showcase SEM images and the corresponding EDS data for Dy^{3+}-doped phosphor nanoparticles (1.5 wt%) and their dispersion within the 7BA mixture. The EDS analysis highlights the weight percentages of Zn, P, Dy^{3+}, and O, offering a detailed profile of the elemental distribution in the sample. The SEM results confirm the uniform dispersion of Dy^{3+}-doped phosphor nanoparticles in the 7BA matrix, demonstrating the successful integration of the nanoparticles and reinforcing their potential for optimized functional applications.

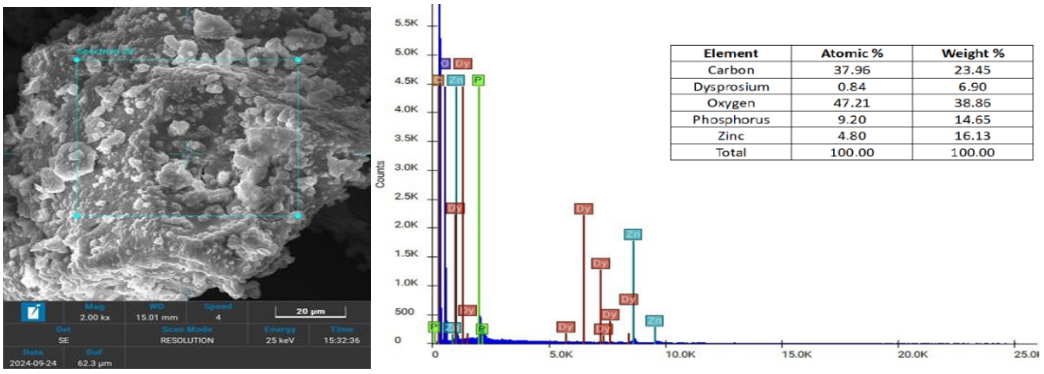

Fig.2(a) SEM & EDS Image of Dysprosium doped lithium zinc phosphate phosphor nano particles

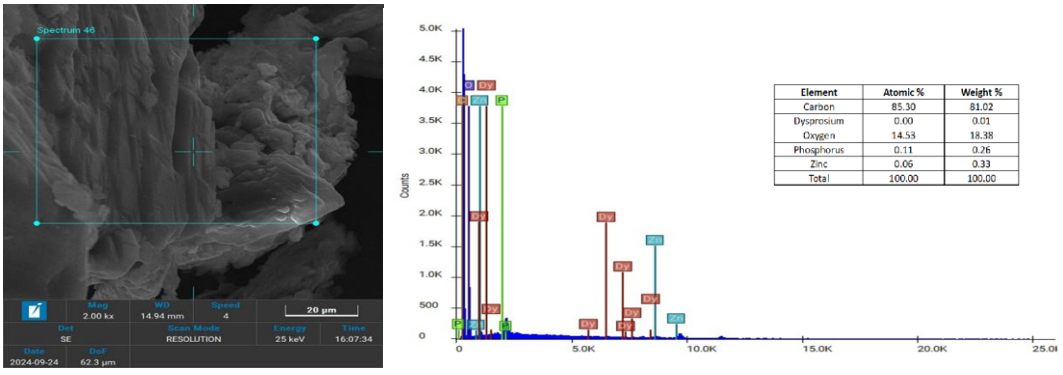

Fig.2(b) SEM & EDS Image of 7BA dispersed with 1.5 wt% Dysprosium doped lithium zinc phosphate phosphor nano particles

3.3 Ultraviolet–visible spectroscopy:

UV-visible spectroscopy, an efficient and non-invasive analytical technique, was employed to examine the absorption characteristics of organic and inorganic samples. The optical properties of liquid crystal-doped nanoparticles at various concentrations were analyzed using a UV-Vis spectrophotometer (Model UV-2450). The absorption spectra for 7BA, doped with Dy^{3+}-doped phosphor nanoparticles at concentrations of 1.5 wt%, 2.5 wt%, and 3.5 wt%, are displayed in Fig. 3(a), covering a wavelength range of 150–400 nm.

The relationship between the absorption coefficient (α) and photon energy (hν) is described by the equation:

$$\alpha h\nu = A(h\nu - Eg)^n$$

where A is a constant, and Eg represents the bandgap energy

The energy bandgap values for the LC 7BA with varying concentrations of Dy^{3+}-doped phosphor nanoparticles (Dysprosium-doped lithium zinc phosphate, $Li_4Zn(PO_4)_2:Dy^{3+}$, abbreviated as DLZ) were derived from the plots of photon energy versus (αhν)2(\alpha hν)^2(αhν)2, as shown in Fig. 3(b). The UV-visible analysis revealed an energy bandgap of 4.04 eV for pure 7BA, which increased to 4.08 eV, 4.11 eV, and 4.13 eV with the addition of 1.5 wt%, 2.5 wt%, and 3.5 wt% Dy^{3+}-doped phosphor nanoparticles, respectively. This indicates that the dispersion of nanoparticles influences the energy distribution of permissible electronic states within the host material, thereby modifying its optical properties.

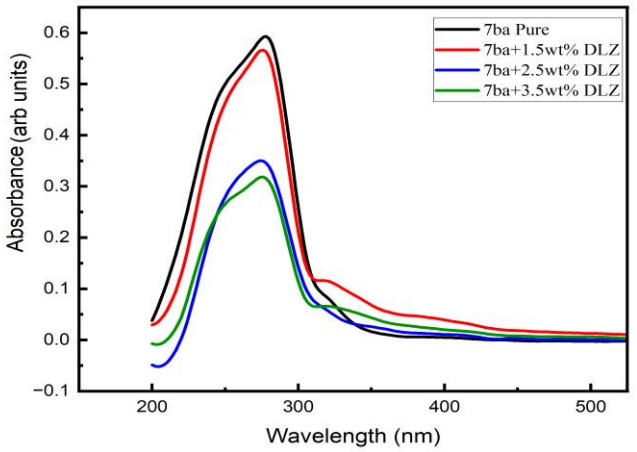

Fig. 3(a) Absorption spectra of 7BA Pure & (1.5-3.5 wt%) dispersed $Li_4Zn(PO_4)_2:Dy^{3+}$ phosphor nps

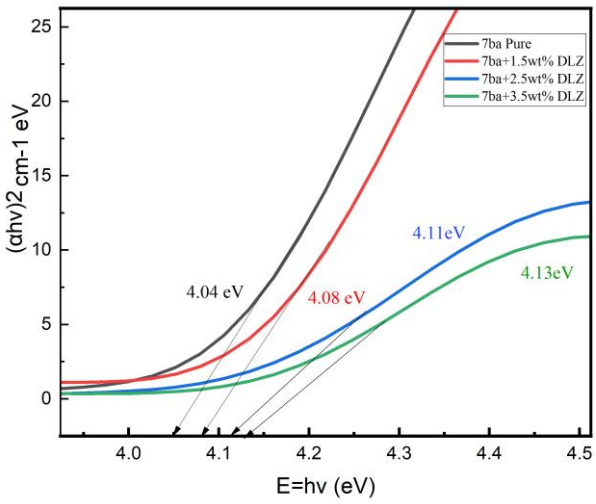

Fig. 3(b) Energy band gap of 7BA Pure & (1.5-3.5 wt%) dispersed $Li_4Zn(PO_4)_2:Dy^{3+}$ phosphor nps

3.4 Differential scanning calorimetry:

Differential Scanning Calorimetry (DSC) is a thermal analysis method designed to measure heat flow associated with phase transitions in materials as a function of temperature and time. This technique offers valuable insights into phase transition temperatures and physical properties such as melting, crystallization, and thermal stability of various compounds. The thermal behavior of liquid crystal-doped nanoparticles at different concentrations was investigated using DSC (Model: STA 7300, Manufacturer: Hitachi, Japan). The phase transition temperatures for pure 7BA liquid crystal, along with those containing Dy^{3+}-doped phosphor nanoparticles at concentrations of 1.5 wt%, 2.5 wt%, and 3.5 wt%, are depicted in Figures 4(a-c).

The DSC-derived transition temperatures closely align with those determined via Polarized Optical Microscopy (POM), with any minor discrepancies attributed to environmental variations. During cooling through the isotropic-nematic (I-N) transition particularly in the fluctuation-dominated nonlinear region (FDLNR)—the liquid crystal molecules lose rotational symmetry and align along a preferred axis known as the director. This molecular realignment causes sudden changes in volume and enthalpy, observed as heat release during cooling and heat absorption during heating. The phase transition temperatures recorded are summarized in Table 1.

S.No	Compound(cooling)	DSC/POM	Transition Temperature (°C)	
			I-N	N-Solid
1	7ba pure	DSC	116.28	96.65/91.5
		POM	116.1	96.5
2	7ba +1.5 wt% Dy^{3+} doped phosphor nps	DSC	117.28	97.25
		POM	117.1	97.1
3	7ba +2.5 wt% Dy^{3+} doped phosphor nps	DSC	118.02	96.05
		POM	118.0	96.0
4	7ba +3.5 wt% Dy^{3+} doped phosphor nps	DSC	119.50	95.50
		POM	118.8	94.8

Table: 1

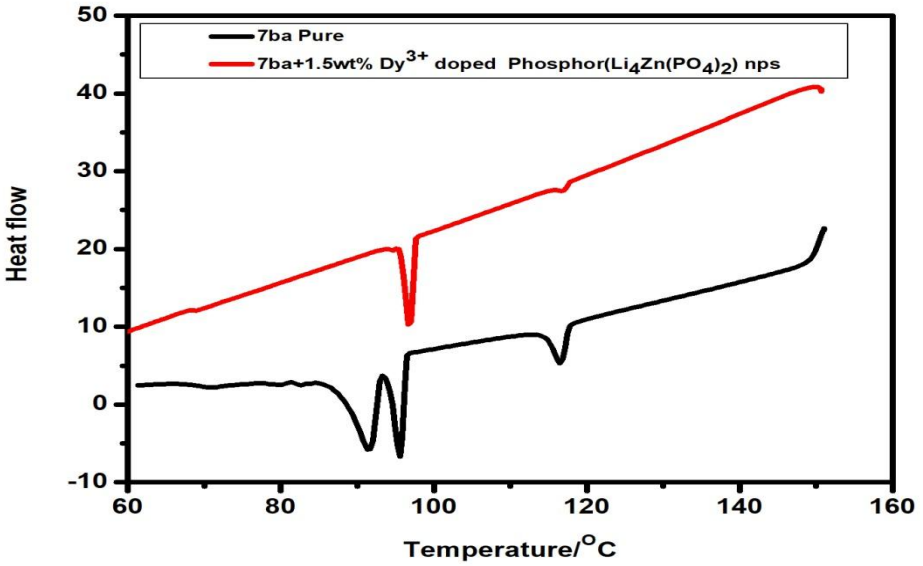

Fig 4(a) DSC Thermograms of Pure 7BA with 1.5 wt% $Li_4Zn(PO_4)_2$:Dy^{3+}

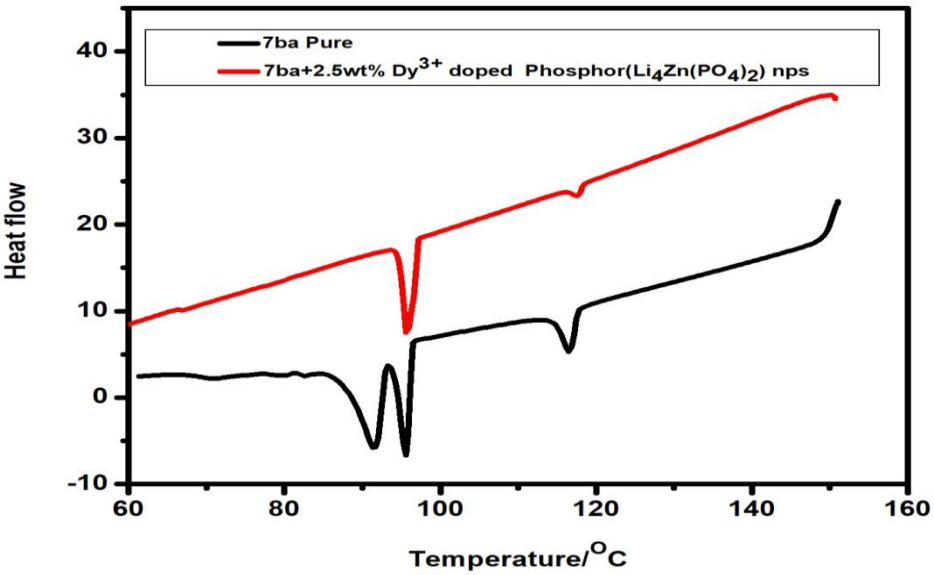

Fig 4(b) DSC Thermograms of Pure 7BA with 2.5 wt% $Li_4Zn(PO_4)_2$:Dy^{3+}

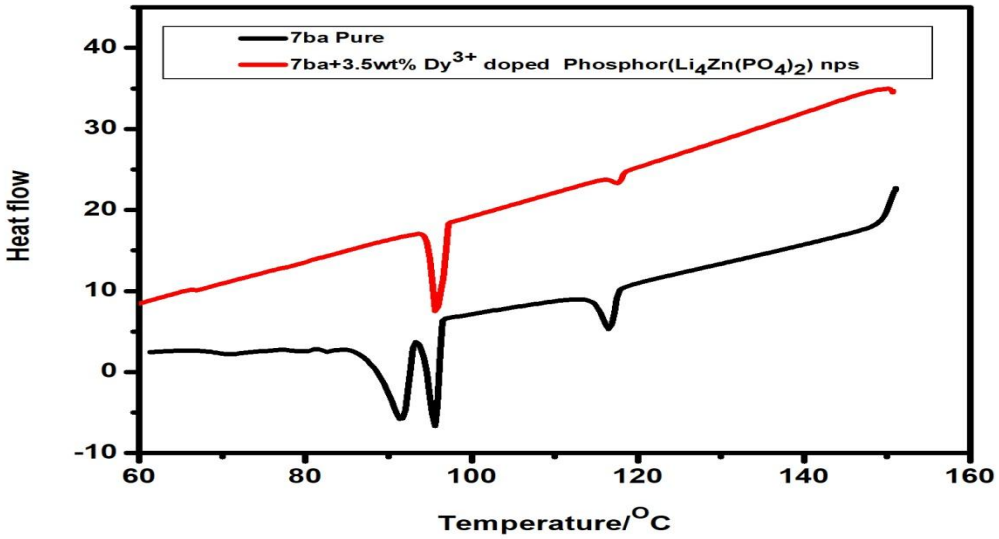

Fig 4(c) DSC Thermograms of Pure 7BA with 3.5 wt% $Li_4Zn(PO_4)_2$:Dy^{3+}

3.5 Polarizing optical microscopy:

A polarizing optical microscope (POM) equipped with a thermal setup was employed to examine the textural characteristics associated with the phase transitions of various liquid crystal (LC) samples. The alignment and texture of liquid crystal-doped nanoparticles at different concentrations were analyzed using a POM (Model: SDTECHS-SDVPM 2727, Manufacturer: SD TECHS). This method provides valuable insights into the isotropic and anisotropic properties of the LC samples, while also identifying their optical behavior as positive or negative. Operating at a 10X magnification, the POM is equipped with a precision-controlled heating block, maintaining a temperature accuracy of ± 0.1°C, regulated through voltage varia.

To conduct the analysis, LC mixtures with varying concentrations of Dy^{3+}-doped phosphor nanoparticles were placed on glass slides, covered with slips, and positioned within the heating block as outlined in [32]. The POM enabled the visualization of diverse textures in the nematic and smectic phases of the LC compounds and their nanocomposites, which arise from changes in the molecular orientational order within localized regions. Commonly, droplet-like and threaded textures were observed in the nematic phase, as illustrated in Figures 5(a-c) and 5(d-f). While the overall LC textures remained largely consistent, a slight influence on the phase transition temperatures was noted due to the dispersion of the nanoparticles.

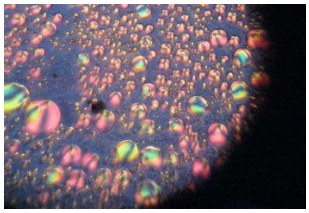

Fig 5(a)
I-N at 116.1ºC

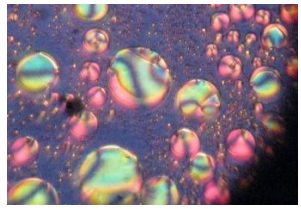

Fig 5(b)
Nematic at 112.2ºC

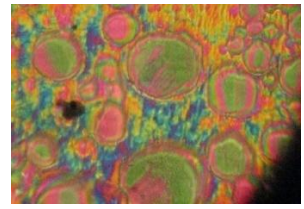

Fig 5(c)
Nematic –Solid at 96.5ºC

Fig. 5(a-c) POM images of Pure 7ba

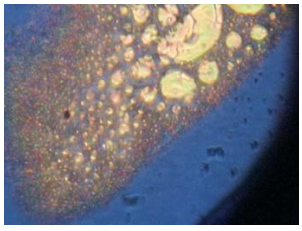

Fig 5(d)
I-N at 117.1ºC

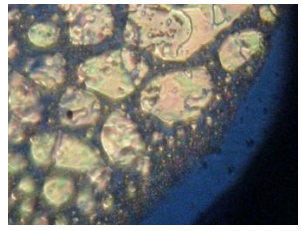

Fig 5(e)
Nematic at 113.4ºC

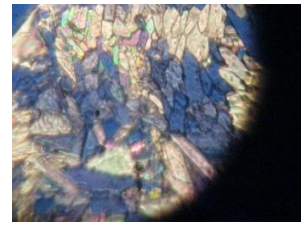

Fig 5(f)
Nematic –Solid at 97.1ºC

Fig. 5(d-f) POM images of 7ba+1.5wt% Dy^{3+} Li_4 $Zn(PO_4)2$ nps

3.6 FTIR Studies:

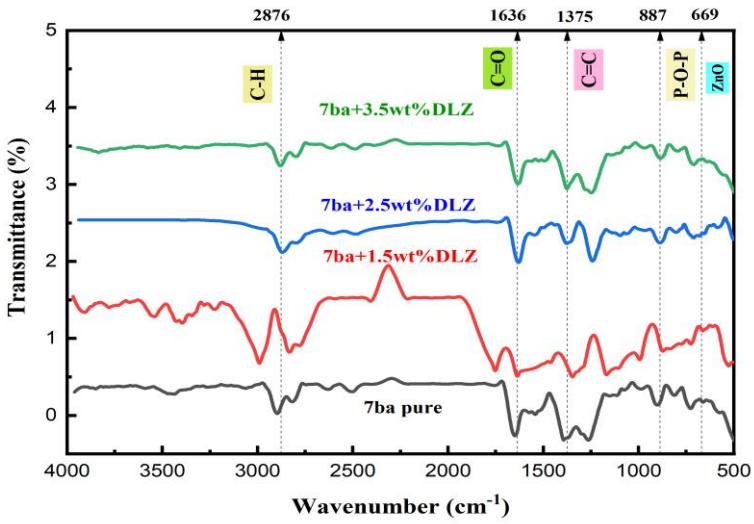

Fig:7 FTIR of 7BA Pure & dispersed (1.5-3.5 wt% $Li_4Zn(PO_4)_2$:Dy^{3+} phosphor nps)

Infrared (IR) spectroscopy is a versatile technique used to identify and characterize organic, inorganic, and polymeric materials by analyzing their chemical properties under IR radiation. When molecular vibrations and rotations interact with electromagnetic radiation, distinct bands appear in the IR spectrum, offering insights into molecular bonding and structure.

The FTIR spectra of 7BA liquid crystal, incorporated with Dy^{3+}-doped phosphor nanoparticles at three weight concentrations (1.5 wt%, 2.5 wt%, and 3.5 wt%), were recorded over the wavenumber range of 500–4000 cm^{-1}, as shown in Fig. 6. The spectrum features five prominent bands at approximately 669 cm^{-1}, 887 cm^{-1}, 1375 cm^{-1}, 1636 cm^{-1}, and 2876 cm^{-1} [33,34].

The band at ~669 cm^{-1} corresponds to Zn–O stretching vibrations, while the ~887 cm^{-1} band is attributed to the asymmetric stretching of P–O–P linkages [35]. These bands collectively confirm the presence of PO_4 tetrahedral structures with specific bonding configurations [36,37]. At mid-to-low frequencies, the spectrum reveals a complex profile with contributions from the stretching of carbonyl groups (ν(C=O)) at ~1636 cm^{-1} and aromatic ring vibrations [38]. Additionally, a peak at ~1375 cm^{-1} arises from the stretching of C=C double bonds [39].

The high-frequency region of the spectrum is dominated by strong C–H and O–H stretching vibrations. Beneath the prominent ν(C–H) peaks near ~3000 cm^{-1}, a broad feature attributed to the Fermi A-type band is observed, corresponding to the fundamental O–H stretching vibration, peaking around ~2876 cm^{-1} [40,41].

With increasing nanoparticle concentration, noticeable shifts in wavenumbers associated with the anomalous stretching of C=O, C=C, and C–H bonds are observed. These shifts highlight the dynamic interaction between the liquid crystal matrix and the dispersed nanoparticles. Vertical dashed lines in the spectrum mark the characteristic vibrational signatures of the

liquid crystal-nanoparticle composites, serving as benchmarks for comparative analysis.

4. Conclusion:

The optical and spectral characteristics of p-(n-heptyl) benzoic acid (7-BA) liquid crystal (LC) compounds doped with dysprosium-doped lithium zinc phosphate phosphor nanoparticles at varying concentrations (1.5 to 3.5 wt.%) were explored using a range of experimental techniques, including XRD, SEM, UV-Vis spectroscopy, DSC, POM, and FTIR spectroscopy. X-ray diffraction (XRD) confirmed the successful integration of the nanoparticles, revealing an estimated crystallite size of 88 nm. Surface morphology and elemental composition of the dysprosium (Dy), zinc (Zn), and phosphorus (P) nanoparticles within the LC matrix were examined through SEM-EDS analysis. UV-Vis spectroscopy showed a decrease in absorbance upon nanoparticle dispersion in the 7-BA LC compound, thereby increasing the energy gap. Phase transitions were monitored using differential scanning calorimetry (DSC) and polarized optical microscopy (POM), with results showing slight temperature fluctuations, likely due to environmental factors, while remaining consistent across measurements. FTIR spectroscopy identified the functional groups present in the LC system and detected minor shifts in wave numbers, attributed to the integration of the nanoparticles.

The incorporation of dysprosium-doped lithium zinc phosphate phosphor nanoparticles into 7-BA liquid crystal compounds significantly enhanced their optical, structural, and thermal properties. The nanoparticles decreased absorbance, altered phase transition behavior, and introduced minor shifts in functional group vibrations, making these materials promising for display and optoelectronic applications. Future work will focus on exploring other liquid crystal systems and studying their dielectric properties for advanced electronic devices.

Acknowledgment

The authors thank Advanced Analytical Laboratory, Andhra University, and GITAM University, Visakhapatnam for providing characterization facilities.

Role of the funding sources: This article's work has no funding sources.

Conflict of Interest: The authors declare that there is no conflict of interest regarding the publication of this paper.

References

1 Yuriy Garbovskiy and Iryna Glushchenko , Crystals 5, 501-533; doi:10.3390/cryst5040501 (2015)
2 Amit Choudhary, Gautam Singh and Ashok M. Biradar, Nanoscale , 6, 7743(2014) DOI: 10.1039/c4nr01325e
4 S. T. Wu, Q. T. Zhang, S. Marder, Jpn. J. Appl. Phys., 37, L1254–L1256 (1998).
5 G. K. Auernhammer, J. B. Zhao, D. Ullrich Vollmer, Eur. Phys. J. E., 30, 387–394 (2009).
6 D. Sikharulidze, Appl. Phys. Lett., 86, 033507 (2005).
7 T. Hegmann, H. Qi, B. Kinkead, V. M. Marx, H. Girgis, P. A. Heiney, Can. J. Met. Mater. Sci., 48, No.1, 1–8 (2009).
8 P. Martinot-Lagarde, G. Durand, J. Phys., 42, 269–275 (1981).
9 M. Rahman, W. Lee, J. Phys. D: Appl. Phys., 42, 063001 (2009).

10 A. K. Misra, A. K. Srivastava, J. P. Shukla, R. Manohar, Phys. Scr., 78, 065602 (2008).
11 J.P.F. Lagerwall, and G. Scalia, Curr. Appl. Phys., 12, 1387–1412 (2012), doi.org/10.1016/j.cap.2012.03.019
12 O. Stamatoiu, J. Mirzaei, and X. Feng, Top Curr. Chem., 318, 331–394 (2012). doi.org/10.1007/128_2011_233
13 M. Gao, K. Li, Y. Yan, S. Xin, H. Dai, G. Zhu, and C. Wang, J. Mol. Struct., 1228, 129471 (2021).doi.org/10.1016/j.molstruc.2020.129471
14 L. Yu, H. Song, Z. Liu, L. Yang, and S.L.Z. Zheng, J. Phys. Chem. B, 109, 11450–11455 (2005). doi.org/10.1021/jp045238e
15 Rita A. Gharde, Madhavi S. Pradhan, Santosh A. Mani, Jyoti R. Amare, International Journal of Chemical and Physical Sciences. Vol. 3, April- 2014, Special issue NCRTSM, ISSN:2319-6602, https://www.ijcps.org/0Site/SP2/P12.pdf
16 Porov, Preeti , Chandel, Vishal Singhmm , Manohar, Rajiv, Transactions on Electrical and Electronic Materials, Volume 17 Issue 2 / Pages.69-78 / 2016 / 1229-7607(pISSN)
17 R Carey, P A Gago-Sandoval, D M Newman and B W J Thomas, Measurement Science and Technology, 7(4),1996,p505, DOI 10.1088/0957-0233/7/4/006
18 Volodymyr Tkachenko, Antigone Marino, Giancarlo Abbate, Society for Information Display 18(11), November 2010,Pages 896-903, https://doi.org/10.1889/JSID18.11.896
19 V. Tkachenko, A. Marino, F. Vita, F. D'Amore, L. De Stefano, M. Malinconico, M. Rippa, and G. Abbate, Eur. Phys. J. E 14, 185–192 (2004),
20 Keisuke Ito , Kazuya Goda, Munehiro Kimura, and Tadashi Akahane Japanese Journal of Applied Physics 50 (2011) 01BB02, DOI: 10.1143/JJAP.50.01BB02
21 Y.A. Garbovskiy, A.V. Glushchenko, Liquid crystalline colloids of nanoparticles
22 J.P.F. Lagerwall, G. Scalia, Liquid Crystals with Nano and Microparticles World Scientific Publishing Co. Pte Ltd., Singapore (2017) Ltd., Singapore (2017).
23 Gao, M.; Li, K.; Yan, Y.; Xin, S.; Dai, H.; Zhu, G.; Wang, J. Mol. Struct, 1228,(2021) doi.org/10.1016/j.molstruc.2020.129471
24 Akinapally Naveen ,M Venkateswarlu ,M V V K Srinivas Prasad, Nakka Chandana ,Biointerface Research in Applied Chemistry, Volume 14, Issue 3, 65(2024)
25 J. C. Nie, J. Y. Yang, Y. Piao, H. Li, Y. Sun, Q. M. Xue, C. M. Xiong, R. F. Dou, and Q. Y Tu, Appl. Phys. Lett., 93, No. 17, 173104 (2008).
26 B. D. Viezbicke, S. Patel, B. E. Davis, D. P. Birnie, Phys. Status Solidi B, 252, No. 8, 1700–1710 (2015).
27 D. Newbury, D. C. Joy, P. Echlin, C. E. Fioriand, and J. I. Goldstein, Advanced Scanning Electron Microscopy and X-Ray Microanalysis, Plenum Press, New York (1986).
28 P. Jayaprada, M. C. Rao,B. T. P. Madhav, and R. K. N. R. Manepalli, DOI :10.1007/s11182-024-03182-5
29 Maria Losurdo Æ Michael Bergmair Æ Giovanni Bruno Æ Denis Cattelan Æ, J Nanopart Res 11:1521–1554(2009)
30 Neeraj , Pankaj Kumar , K.K. Raina, Optical Materials, Volume 34, Issue 11, Pages 1878-1884 (2012)
31 S. Delice , M. Isik , N.M. Gasanly , N.H. Darvishov , V.E. Bagiev, Optik,Volume, 262, July 2022
32 V Balasubramanian, V N Vijayakumar, T Vasanthi,Brazilian Journal of Physics, 53:36(2023)
33 H.S. Liu, T.S. Chin, S.W. Yung, Mater. Chem. Phys. 50, 1–10 (1997)
34 J.O. Byun, B.H. Kim, K.S. Hong, H.J. Jung, S.W. Lee, A.A. Izyneev, J. Non Cryst. Solids, 190, 288–295, (1995)
35 M. Shwetha , B. Eraiah, Journal of Non-Crystalline Solids,Volume 555,1206221 March(2021)

https://doi.org/10.1016/j.jnoncrysol.2020.120622
36 Debnath, S.; Saxena, S.K.; Nagabhatla, V. Catal. Commun. 84, 129–133,(2016) https://doi.org/10.1016/j.catcom.2016.06.018.
37 Lai, Y.M.; Liang, X.F.; Yang, S.Y.; Wang, J.X.; Cao, L.H.; Dai, B. J. Mol. Struct., 992, 84–88, (2011) https://doi.org/10.1016/j.molstruc.2011.02.049.
38 Johnson SL, Rumon KA.. J Phys Chem.,69(1):74(1965). doi:10.1021/j100885a013.
39 K. Sankarranarayanan, C. Kavitha, M.L.N. Madhu Mohan PII: Optik Volume 143, Pages 42-58August (2017) DOI: http://dx.doi.org/doi:10.1016/j.ijleo.2017.06.047
40 Lee JY, Painter PC, Coleman MM. Macromolecules.;21(4):954–960(1988).. doi:10.1021/ ma00182a019
41 Kato T, Wilson PG, Fujishima A, et al. Chem Lett. 1990;11:2003–2006. doi:10.1246/ cl.1990.2003.